Available online at www.sciencedirect.com

SciVerse ScienceDirect

journal homepage: www.elsevier.com/locate/he

Enhanced photocatalytic water splitting activity of carbon-modified TiO_2 composite materials synthesized by a green synthetic approach

Sreenivasan Koliyat Parayil [a], *Harrison S. Kibombo* [a], *Chia-Ming Wu* [a], *Rui Peng* [a], *Jonas Baltrusaitis* [b], *Ranjit T. Koodali* [a,*]

[a] *Department of Chemistry, University of South Dakota, 414 E. Clark Street, Vermillion, SD 57069, USA*
[b] *Department of Chemistry, University of Iowa, Iowa City, IA 52246, USA*

ARTICLE INFO

Article history:
Received 16 January 2012
Received in revised form
9 February 2012
Accepted 11 February 2012
Available online 13 March 2012

Keywords:
TiO_2
Sucrose
Pyrolysis
Carbonization
Photocatalysis
Hydrogen evolution

ABSTRACT

We report a green and facile approach for the preparation of carbon-modified (C-modified) TiO_2 composite materials by hydrothermal synthesis followed by pyrolytic treatment. The resultant materials were characterized by powder X-ray diffraction (XRD), nitrogen physisorption studies, Raman spectroscopy, X-ray photoelectron spectroscopy (XPS), diffuse reflectance spectroscopy (DRS), photoluminescence (PL) spectroscopy, and transmission electron microscopy (TEM). The photocatalytic performances of these materials were evaluated by calculating the amount of hydrogen evolved from the decomposition of water under solar simulated irradiation conditions. An improvement was achieved from no H_2 evolution at all with the bare TiO_2, to an evolution of 0.21 mL g^{-1} h^{-1} from a composite material modified with an optimum carbon loading of 3.62%. These results suggested that the interaction of carbon with predominantly rutile form of TiO_2 can promote shallow trapping of photogenerated electrons in the oxygen vacancies. This phenomenon consequently enhances the photocatalytic activity by minimizing charge carrier recombination, a characteristic demonstrated by fluorescence quenching of the TiO_2 emission.

1. Introduction

Hydrogen has emerged as a potential energy carrier in various low greenhouse gas energy applications due to its renewability and innocuity to the environment [1]. Fossil fuels and biomasses are some of the essential sources of hydrogen; however their utilization for energy production is not only capital intensive but also involves the emission of CO_2 that contributes to the adversities of the greenhouse effect and global warming. The generation of hydrogen from water is a more sustainable approach that provides a means through which renewable sources such as solar energy can be harnessed effectively and most importantly this process is carbon neutral, thus preventing environmental pollution. Harvesting of solar energy is still a challenging venture, and the constraints associated to this process necessitate improved methods and advanced technologies for production. The ability of semiconductor materials to utilize photons of light for the generation of electrons and holes has attracted a great deal of attention and has found potential application as photocatalysts [2], solar cells [3], biosensors [4] as well as artificial light harvesting systems [5]. Fujishima and Honda [6] reported

* *Corresponding author*. Tel.: +1 6056776189; fax: +1 6056776397.
E-mail address: ranjit.koodali@usd.edu (R.T. Koodali).
0360-3199/$ – see front matter
doi:10.1016/j.ijhydene.2012.02.067

the photoelectrochemical production of hydrogen from water using TiO_2 electrodes; however the wide band gap of titania limits its application within the UV region. The photocatalytic efficiency is significantly impacted by rapid electron–hole recombination. Thus, one of the goals in this area of research is to develop visible light absorbing photocatalysts that have charge carrier recombination minimized. The photo-excitation of TiO_2 photocatalysts requires light with energy greater or equal to that of its band gap [7] allowing transfer of excited electrons (e^-) to the conduction band, leaving behind positive holes (h^+) in the valence band. These charge carriers can recombine or get trapped in some metastable surface states, and react with electron donors or acceptors. Charge recombination is minimized, and subsequent photocatalytic reactions may occur efficiently on the semiconductor surface when suitable electron donors and/or acceptors are available to interact with the charge carriers. Therefore, electron trapping is a decisive factor in the photocatalytic performance of TiO_2 materials.

It has been determined that hybrid materials of TiO_2 are an ideal choice for controlling the charge separated states [8]. Whereas the structural disorder at the contact between two crystalline nanoparticles leads to enhanced scattering of free electrons and results in reduced electron mobility [9], ordered and strongly interconnected nanoscale architecture offers the potential for improved hole accessibility to acceptors thus contributing to higher photoefficiencies.

Over the past few years, extensive efforts have been directed towards the improvement of visible light sensitivity of TiO_2. Substitution of metal ions in TiO_2 has been proven to be effective in improving photocatalytic efficiency, however mixed results have been obtained [10,11]. In this respect, non-metal modifications have been touted as an ideal and inexpensive choice for narrowing the band gap and increasing the visible light response of wide band gap semiconductors. To date, there are numerous literature related to the incorporation of non-metal atoms such as boron [12], fluorine [13], iodine [14], nitrogen [15,16], sulfur [17,18], and carbon [19,20].

Despite the complexities in synthetic procedures, the use of C-modified TiO_2 has been studied extensively [21,22]. Khan et al. [21] verified the high photoactivity of C-doped TiO_2 in the photoelectrochemical water splitting reaction to produce H_2 and O_2, and obtained photo-conversion efficiencies as high as 8.35%. Similarly, Park et al. [22] showed that TiO_2-carbon nanotube composite arrays provide efficient photoelectrochemical water splitting efficiencies under visible light than pure nanotube arrays. Chen et al. [23] compared the visible light photocatalytic degradation of methylene blue (MB) using C-doped, N-doped, and C–N co-doped TiO_2 nanoparticles prepared by sol–gel method and determined that band gap narrowing led to substantially higher photocatalytic activity. Sakthivel et al. [24] determined that C-doped TiO_2 is five times more active than N-doped counterparts in the degradation of 4-chlorophenol under visible light. Janus et al. [25] utilized the carbonization of alkanes at high temperature to demonstrate that the visible light activity of such C–TiO_2 composites is strongly dependent on the nature of carbon.

New methods have been adopted to simplify the synthetic procedures and improve the quality of the resultant materials. Gu et al. [26] proposed a facile template-free preparation of micro-mesoporous C-doped TiO_2 using a low temperature procedure that involved the dispersion of TiC in nitric acid and ethanol, followed by heating to 60 °C, and drying at 120 °C. Also, Kim et al. [27] have recently explored a novel synthesis route for the preparation of C-TiO_2 by using high energy electron beam irradiation to induce surface doping into greater portions of the semiconductor material.

Environmentally friendly biomass and simple sugars such as glucose and sucrose have shown to impart carbonaceous properties on TiO_2 nanoparticles and improve overall photocatalytic activities. Dong et al. [28] prepared C-doped TiO_2 by hydrothermal treatment of titanium sulfate with glucose and evaluated the visible light photoactivity for degradation of toluene in the gas phase. In a subsequent work, the C-doped TiO_2 nanoparticles were subject to calcination in air at different temperatures [29]. The post-thermal treatment led to materials with less surface defects and an enhancement in the photocatalytic activity was observed. Zhang et al. [30] prepared C-modified titania *via* a two-step approach. In their method, a commercial sample of titania (Degussa P25) was subjected to carbonization *via* a hydrothermal method using glucose. In the final step, graphitization was carried out by heating to 800 °C in N_2 atmosphere.

Recently Zhao et al. [31] reported furfural as the modifier for the synthesis of C-doped TiO_2 for degradation of methyl orange (MO). They treated furfural with titanium isopropoxide in alcohol media and observed that the presence of the alkoxide permits the co-assembly of carbon and TiO_2 in an interpenetrating C/TiO_2 nano-architecture containing 12.6% carbon. Recently Li et al. [32–36] explored possible means through which hydrogen could be evolved photocatalytically from TiO_2 using oxalic acid as an electron donor [32], dye sensitization [33], and by co-doping [34]. In this respect, they also attempted to study visible light sensitivity of CdS nanostructures and observed high hydrogen evolution [35,36]. Although there are numerous literatures related to the synthesis of carbonaceous TiO_2 materials from biomass such as glucose, furfural etc., photocatalytic evolution of hydrogen from photosplitting of water has not been attempted in detail. This manuscript addresses the carbonization of TiO_2 by pyrolysis, and their effect on the photocatalytic evolution of hydrogen under solar simulated conditions is explored. This one-pot approach provides a highly economical and green synthetic pathway that obviates the use of toxic organic solvents, and provides new information relevant to practitioners in the broad area of sustainable solar energy conversion.

2. Experimental

2.1. Materials

Commercially available titanium isopropoxide, $Ti(OPr^i)_4$ (Acros, 98%), ethanol, (Pharmco-AAPER, A.C.S./USP grade, anhydrous), conc. HNO_3 (Acros, ACS grade), methanol (Acros, 99.9% HPLC grade), and sucrose (Fisher scientific) were used as received. Deionized water (resistivity >18 Ω m) was used throughout the experiments.

2.2. Synthesis of TiO_2–Sucrose composites

In a typical synthesis, 2.2 mL of $Ti(OPr^i)_4$ was added drop wise to a solution containing 9 mL of C_2H_5OH under vigorous stirring in a Teflon liner. The hydrolysis process was initiated by the introduction of 1 mL of H_2O and catalyzed by the addition of 100 μL of conc. HNO_3 during stirring. A required amount of sucrose solution was added and the mixture was stirred until gelation, which was usually achieved within 3 h. The resultant gels were subjected to hydrothermal treatment in a Thermolyne autoclave reactor furnace, and heated to a temperature of 120 °C for 14 h, filtered, and dried overnight at 75 °C. The obtained powders were then ground and subjected to pyrolysis.

2.3. Pyrolytic synthesis for C-modified TiO_2 composites

The incorporation of carbon onto the TiO_2 matrix was performed using sucrose as the carbon precursor. The above-synthesized composite powders were transferred to a ceramic boat, placed in a tubular furnace, purged with N_2 gas, and heated at 800 °C at a rate of 10 °C/min for 4 h and the cooled gently. It was determined that control of the temperature and N_2 flow rate was critical for effective carbonization of the composite mixture. The resultant materials were denoted as, TiO_2-C-79, TiO_2-C-120, TiO_2-C-362, and TiO_2-C-402, where the values indicate the percentages of carbon present in each of the sample after pyrolysis, i.e. 0.79, 1.20, 3.62 and 4.02%, and confirmed by Elemental Analysis. A control material was prepared without the addition of sucrose in order to study the effect of carbonization. After the hydrothermal reaction, the TiO_2 powder was calcined and pyrolyzed at 800 °C in air and N_2 atmosphere to obtain TiO_2-0 and TiO_2-0-N respectively.

2.4. Catalyst characterization

The samples were characterized by transmission electron microscopy (TEM), powder X-ray diffractometry (XRD), Raman spectroscopy, UV–Visible diffuse reflectance spectroscopy (DRS), and photoluminescence (PL) spectroscopy. TEM images were recorded on a Tecnai G^2 instrument operating at 120 kV. For the preparation of sample for TEM analysis, TiO_2-C-79 was dispersed in ethanol, and the suspension was sonicated for 1 h. One drop of the suspension was placed on a TEM grid, and allowed to dry overnight. The powder XRD measurements were performed at room temperature using a Rigaku Ultima IV X-ray diffractometer with Cu Kα radiation. The diffractometer was operated at 40 kV and 44 mA and scanned with a step size of 0.02° at a scan speed of 1°/min in the range of $2\theta = 10–80°$. The UV–Vis diffuse reflectance spectra were recorded by a Cary 100 Bio UV–Visible spectrophotometer with a praying mantis diffuse reflection accessory (Harrick Scientific). Raman spectra were measured on a Horiba Jobin Yvon Labram Aramis Raman spectrometer with a He–Ne laser (532 nm) as the light source. The unfiltered beam of scattered laser radiation was focused onto the sample through a microscope objective (×50) for an acquisition time of 10 s and repetition of 10×. The radiation was then dispersed by an 1800 line/mm grating onto a CCD detector. X-ray photoelectron spectroscopy was carried out using a custom-designed Kratos Axis Ultra instrument in a surface analysis chamber with monochromatic radiation at 1486.6 eV from an aluminum K_α source using a 500 mm Rowland circle silicon single crystal monochromator. The X-ray gun was operated with current at 15 mA and at an accelerating voltage of 15 kV. Low energy electrons were used for the charge compensation to neutralize the samples. Samples were transferred to the indium foil and mounted on to the copper stub. Survey scans were collected by using the following instrument parameters: energy scan range of 1200 to −5 eV, pass energy of 160 eV, step size of 1 eV, dwell time of 200 ms, and an X-ray spot size of 700 × 300 μm. High resolution spectra were acquired in the region of interest using the following experimental parameters: 20–40 eV energy window, pass energy of 20 eV, step size of 0.1 eV, and dwell time of 1000 ms. One sweep was used to acquire a survey spectrum of all binding regions. The absolute energy scale was calibrated to the Cu $2p_{2/3}$ peak binding energy of 932.6 eV using an etched copper plate. All spectra were calibrated using C 1s peak at 284.6 eV, and a Tougaard-type background was subtracted from each spectrum. The textural properties such as surface area and pore size distribution of bare TiO_2 and the C-modified TiO_2 composites were measured using N_2 physisorption measurements. After the samples were dried overnight at 70 °C and degassed at 100 °C for at least 1 h, N_2 isotherms were obtained at 77 K using a NOVA 2200*e* (Quantachrome Instruments) surface area and pore size analyzer. The surface area was calculated by using the Brunauer–Emmett–Teller (BET) equation within a relative pressure range (P/P_0) of 0.05–0.30. The pore volume was determined from the amount of N_2 adsorbed at the highest relative pressure of (P/P_0) ≈ 0.99. The pore diameter and pore size distribution plots were obtained by applying the Barrett–Joyner–Halenda (BJH) equation to the desorption isotherm. PL measurement was carried out on a Horiba Jobin Yvon-Fluoromax4. The excitation wavelength used was 280 nm, and the emission was monitored in the range of 400–600 nm. Elemental analyses were performed on the Exeter Analytical, Inc. CE-440 elemental analyzer manual injection-type configured for the C, H, N modes (oxygen combustion oven at 980 °C and copper reduction oven at 700 °C).

2.5. Photocatalytic water splitting

Photocatalytic hydrogen evolution reactions were carried out in a 5 mL quartz reactor similar to a previous study carried out by our group [37]. Typically 2 mg of the catalyst was suspended in a solution of 1.6 mL of H_2O and 0.4 mL of methanol. A 300 W Xenon lamp equipped with an optical transmission filter >280 nm was used as the AM 1.5 simulated light source. The suspension was degassed for 30 min. with high-purity argon prior to light irradiation in order to eliminate dissolved oxygen. The amount of H_2 produced was measured by gas chromatography (SRI 8610C) equipped with a molecular sieve column and a TCD detector, and using a previously prepared calibration graph.

3. Results and discussion

Various chemical reactions of sucrose can take place under hydrothermal conditions such as hydrolysis of the sugars to

monomers, polymerization and condensation of soluble products, and subsequent nucleation of aromatic clusters as the solution reaches a critical super saturation point [38]. No carbonization takes place when sucrose solution was treated with TiO_2 precursor solutions at room temperature. However, the appearance of an orange-brown color after the hydrothermal treatment indicate that oligosaccharides and charge transfer complexes were formed due to polymerization of monosaccharides [39]. The carbonization step may arise from a cross-linking process induced by intermolecular dehydration of linear or branchlike oligosaccharides, or other macromolecules formed during pyrolysis. The resulting complex then stacks together to form carbon layers in which TiO_2 is likely to be anchored to the surface [40,41].

3.1. *Powder X-ray diffraction studies*

The C-modified TiO_2 composites prepared in this study demonstrated highly crystalline rutile TiO_2 in co-existence with small amounts of anatase phase as illustrated by the powder XRD diffraction pattern in Fig. 1. The samples exhibit diffraction peaks due to d_{101}, d_{004}, d_{200}, d_{105}, and d_{204} at two theta values of 25.2°, 37.9°, 48.1°, 55.1°, and 62.8° respectively, indicative of the anatase phase. Rutile peaks due to d_{110}, d_{101}, d_{200}, d_{111}, d_{210}, d_{211}, d_{220}, d_{002}, d_{110}, d_{301}, and d_{112} are at two theta values of 27.5°, 36.1°, 39.2°, 41.23°, 44.2°, 54.3°, 56.7°, 62.9°, 64°, 68.9°, and 69.8° respectively. The amount of anatase content was determined to be 5, ~0, 3, 4, 8, and 1% in the TiO_2-0, TiO_2-0-N, TiO_2-C-79, TiO_2-C-120, TiO_2-C-362, and TiO_2-C-402 samples respectively. It was reported earlier that the carbon diffraction peak may not be observed distinctly owing to small amorphous carbon species attached on the highly crystalline rutile TiO_2 [42], which evokes an investigation into the effect of carbon on the porosity of the TiO_2.

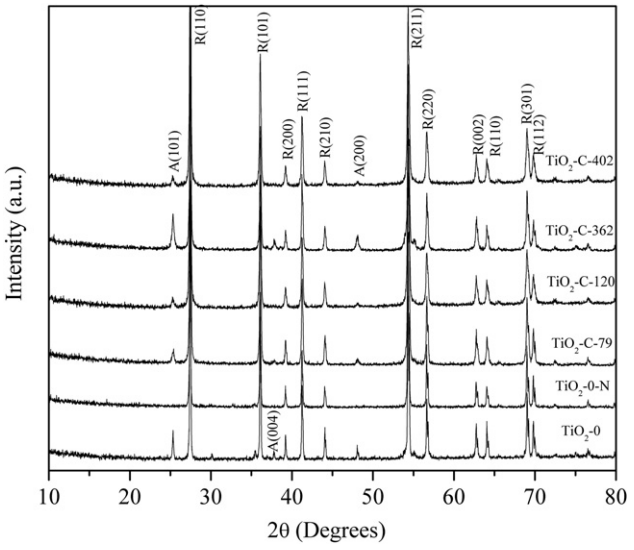

Fig. 1 – Powder X-ray diffraction pattern of C-modified TiO_2 composite material obtained from the pyrolysis of TiO_2 and sucrose. Bare TiO_2-0 and TiO_2 pyrolyzed under N_2 atmosphere (TiO_2-0-N) are also shown for comparison. A and R refers to the anatase and rutile phases of TiO_2 respectively.

3.2. *N_2 physisorption studies*

Fig. 2A exhibits isotherms that provide information about the structural properties and pore geometries of the C-modified TiO_2 composites prepared at various sucrose compositions of 0.79, 1.20, 3.62, and 4.02% carbon. The N_2 isotherms of bare TiO_2 calcined in air (TiO_2-0), and the materials of low carbon content such as TiO_2-C-79 and TiO_2-C-120 showed typical type IV isotherms of mesoporous materials that initially experience monolayer adsorption at low relative pressure (P/P_0) levels up to 0.4. As the relative pressure increases, a steep rise in the isotherm is observed, indicative of multilayer adsorption that precedes capillary condensation. An increase in the carbon loading to 3.62 and 4.02% however, results in materials of type V isotherms exhibiting convexity, a feature that suggests relatively stronger lateral interactions between adsorbed N_2 molecules than the interactions between the adsorbent surface and adsorbate [43]. The pore size characteristics for these materials illustrated in Fig. 2B vary, with TiO_2-0 displaying unimodal distribution centered at 37 Å, indicative of mesoporosity. The distribution of pores is increased as more carbon is introduced in the TiO_2 matrix

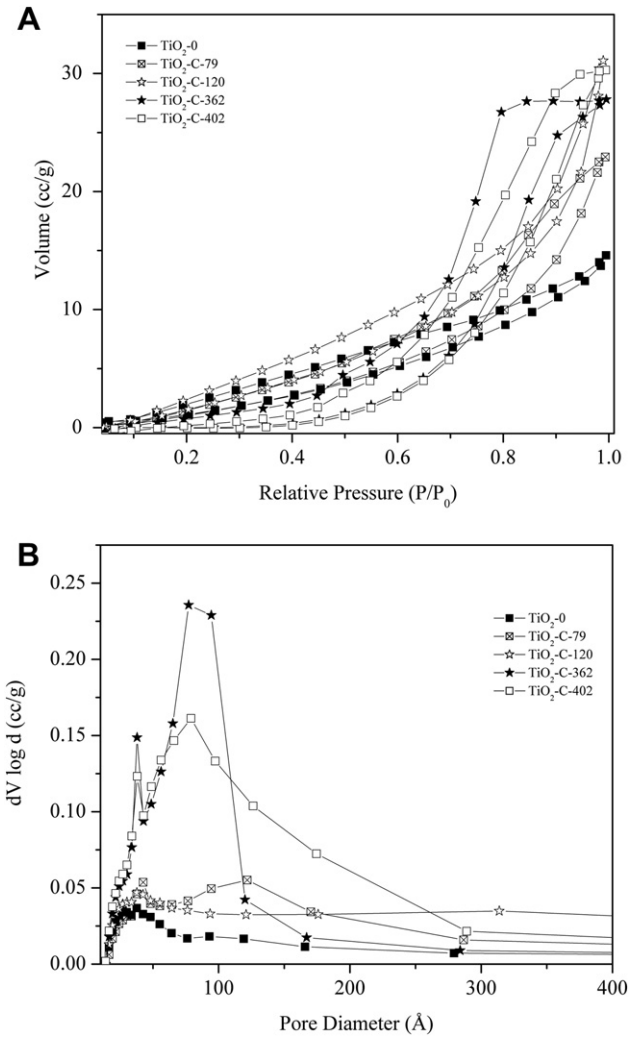

Fig. 2 – Nitrogen physisorption isotherms (A) and pore size distribution (B) of C-modified TiO_2 composites materials.

with bimodal distributions centered at 43 and 121 Å for TiO_2-C-79, whereas TiO_2-C-362 and TiO_2-C-402 exhibited sets of pores in the range of 38 and 78 Å. The difference in pore geometries resulted in differences in surface areas obtained. TiO_2-0 resulted in a material of small surface area of 6.5 $m^2 g^{-1}$, suggesting significant agglomeration of the titania particles because of the high temperature used for calcination. However, the surface areas improved more than 10 times after the carbon modification to values as large as 72 $m^2 g^{-1}$ similar to previously published reports [44,45]. The data related to surface area, pore volume, and average pore diameter obtained from N_2 adsorption–desorption analysis are summarized in Table 1.

3.3. TEM analysis

The morphological properties of the composites prepared in this study were investigated by collecting TEM images of a representative material, TiO_2-C-79, as shown in Fig. 3. The TEM image shows lattice fringes due to TiO_2. The rutile phase with *d* spacing of 3.25 Å due to (110) could be observed in the TEM image. In addition, amorphous carbon layers that were randomly deposited are also observed. The absence of graphitic like carbon species in the TEM studies spurred an investigation into the different types of carbon present in our materials using a characterization technique that is more sensitive to carbonaceous species.

3.4. Raman spectroscopic studies

Owing to the absence of characteristic peaks due to carbon in the powder XRD diffraction patterns and lack of evidence for graphitic layers in TEM, Raman spectra were recorded to confirm the structural features of the composite materials as illustrated in Fig. 4. All the materials exhibited four modes assigned to TiO_2 resulting from phase transformations from anatase to rutile. The bare TiO_2-0 is shown in the inset for comparison. The material possesses an intense peak at 140 cm^{-1} corresponding to the anatase phase and the bands at 235, 450, and 610 cm^{-1} are assigned to the rutile phase, these are consistent with the XRD studies which indicate the presence of rutile phase in large amounts and anatase phase in minor amounts. However, the structural features change as more carbon is incorporated to the composite materials. The first order spectra highlight unique features of carbonaceous materials exhibiting two broad and strongly overlapping peaks with intensity maxima close to 1350 cm^{-1} (D band), related to imperfections in the carbon structure and associated with A_{1g} symmetry. The G band attributed to the E_{2g} vibrational mode of sp^2 bonded carbon atoms is observed at approximately 1585 cm^{-1}. The second order spectra of the composites also exhibits two broad peaks at nearly 2720 and 2950 cm^{-1}assigned to the first overtone of D band (D′) and to a combination of D and G modes respectively characteristic of allotropic forms of carbon structures [46]. The position and intensity ratio of these two bands were hardly altered by increasing the carbon content. This might be due to the formation of amorphous carbon on the surfaces of TiO_2 nanoparticles *via* formation of sucrose–TiO_2 surface complexes. It is noteworthy that vibrational features appearing at wavenumbers above 600 cm^{-1} reveal the identity of the carbonaceous materials that were not observed for the bare TiO_2-0.

3.5. XPS analysis

XPS was used to investigate the surface composition of C-modified TiO_2 materials. The peaks from C 1s, Ti 2s, Ti 2*p*, O 1s, and O auger that were detected in the survey scan from the surface of bare TiO_2-0 and TiO_2-C-362 are shown in Fig. 5A. The high resolution XPS spectrum of Ti 2*p* regions is shown in Fig. 5B. Two intense peaks at 458.7 eV and 464.5 eV were observed for TiO_2-C-362 and TiO_2-0, corresponding to the Ti $2p_{3/2}$ and Ti $2p_{1/2}$ binding energy region, which indicates the presence of Ti^{4+} ions as in TiO_2. Furthermore, Fig. 5C displays spectra corresponding to O 1s region for both of these materials. They reveal the presence of three peaks corresponding to Ti–O bond (530.0 eV), O–H bond (531.4 eV), and C–O bond (532.5 eV) respectively. The C 1s spectra of TiO_2-C-362 and TiO_2-0 are also shown in Fig. 5D. A deconvolution procedure was applied to obtain additional information regarding the different bonding characteristics of carbon. The peak at 284.6 eV is assigned to the C–C neutral bond whose large intensity is a depiction of carbon loaded onto TiO_2 rather than due to adventitious carbon in the TiO_2-C-362 sample. In the sample, TiO_2-0, this peak is less pronounced and thus the peak at 284.6 eV is most likely due to adventitious carbon. This is supported by the fact that elemental analysis of this sample

Table 1 – Textural properties of C-modified TiO_2 composite materials.

Materials	S_{BET}[a] ($m^2 g^{-1}$)	Pore volume ($cm^3 g^{-1}$)	Ave. pore diameter (Å)	BJH[b] pore diameter (Å)	H_2 evolution[c] ($mL/h/g_{TiO2}$)
TiO_2-0	6.5	0.02	133	24	0
TiO_2-C-79	47	0.05	122	25	0.05
TiO_2-C-120	48	0.04	96	43	0.10
TiO_2-C-362	72	0.12	64	38	0.21
TiO_2-C-402	65	0.11	64	38	0.05

a Surface area determined by applying Brunauer–Emmett–Teller (BET) equation to a relative pressure (P/P_0) range of 0.05–0.35 of the adsorption isotherm.
b Calculated from the Barrett–Joyner–Halenda (BJH) equation using the desorption isotherm.
c Values depict photocatalytic efficiencies after 6 h under solar simulated irradiation conditions.

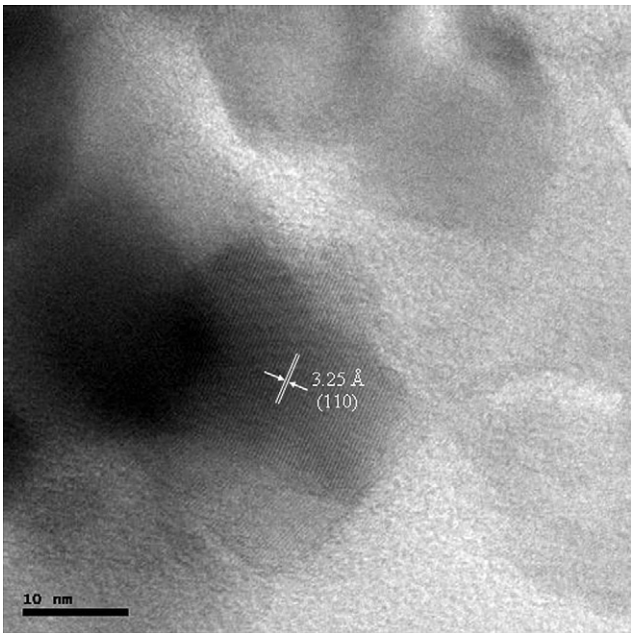

Fig. 3 – TEM image of a representative of the C-modified TiO_2 composites, TiO_2-C-79. TiO_2 nanoparticles are observed as lattice fringes.

resulted in no detection of C. The peaks at 286.1 and 287.6 eV in TiO_2-C-362 are due to C–O and C=O bonds which are formed during the pyrolysis of sucrose and due to non- or partially dehydrated carbohydrate species. In TiO_2-0, these peaks appear at 286.1 and 288.4 eV respectively and are due to the formation of surface carbonate species. Besides these regions, TiO_2-C-362 showed two peaks with low intensities at 289.1 and ~291.4 eV corresponding to the O–C=O binding energy and $\pi-\pi^*$ shake up satellite peak [47] that have been reported for graphite like carbon species [48,49].

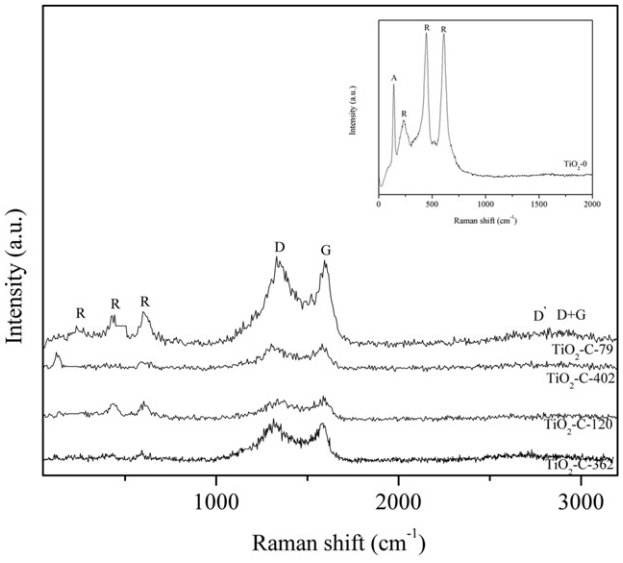

Fig. 4 – Raman spectra of C-modified TiO_2 composites. Bare TiO_2 (TiO_2-0) is also shown for comparison. A and R refers to the anatase and rutile phases of TiO_2 respectively. D, G, D′, D + G refers to the A_{1g}, E_{2g}, first overtone vibration of D band, and combination of D and G mode characteristic of carbon respectively.

3.6. UV–Vis DRS studies

The role of carbonaceous species in the TiO_2 mixed phase materials was further investigated by collecting DRS spectra and these are displayed in Fig. 6A and B. The TiO_2-0 material showed an intense absorption in the UV region (Fig. 6A) and the absorption edge of titania can be easily discerned. The C-modified TiO_2 composites prepared in this study showed similar spectra and enhanced absorption in the visible region in comparison with TiO_2-0. The Fig. 6B shows the Kubelka–Munk plot of the materials prepared in this study. It is evident that TiO_2-0 shows large optical absorbance in the UV region as opposed to the low absorbance demonstrated by C-modified TiO_2 materials. The band gap energy of TiO_2-0 was calculated to be 3.15 eV. However for the carbonized materials, the onset of absorption was extended to the visible region. The wider absorption range for composite materials was attributed to the dark color of the sample.

When TiO_2 was treated with an aqueous solution of sucrose, a color change from white to orange-brown was observed after the hydrothermal treatment but prior to pyrolysis. The complex formed exhibited absorption in the visible light region around 600 nm (not shown). This band is assigned to the ligand-to-metal charge transfer (LMCT) of surface complexes formed between the molecules of sucrose and TiO_2 [50,51]. This optical change is known to be responsible for the excitation of electrons from the chelating ligand (e.g. substrates with hydroxyl or carboxyl binding groups) into the continuum conduction band of TiO_2 nanoparticles as reported by Rajh et al. [52–56].

3.7. Photocatalytic activity of C-modified TiO_2 composite materials

The photocatalytic H_2 evolution results for TiO_2-0, TiO_2-0-N, and C-modified TiO_2 composite materials (TiO_2-C-79, TiO_2-C-120, TiO_2-C-362, and TiO_2-C-402) in aqueous suspension with methanol as sacrificial agent (electron donor) are shown in Fig. 7. The experiments were conducted under solar simulated irradiation (AM 1.5 filter, 300 W m^{-2}) and the results are summarized in Table 1. No H_2 evolution was detected from reactions with bare TiO_2 that was subjected to calcination in air (TiO_2-0) and pyrolysis in N_2 atmosphere (TiO_2-0-N) even after 10 h of irradiation. It has been reported earlier that mixed phases of TiO_2 can generate hydrogen by photocatalytic splitting of water even in the absence of platinum co-catalyst [57], and in some cases, the enhancement due to incorporation of noble metal was minimal [32]. Our results suggest that no hydrogen is evolved for the sample, TiO_2-0. This sample had ~5% anatase; although a mixed phase of anatase and rutile may minimize charge carrier recombination and generate hydrogen, our results indicate the important role that carbon plays in minimizing electron–hole recombination and in producing hydrogen. Based on our results, we can suggest the following mechanism. Upon illumination of TiO_2,

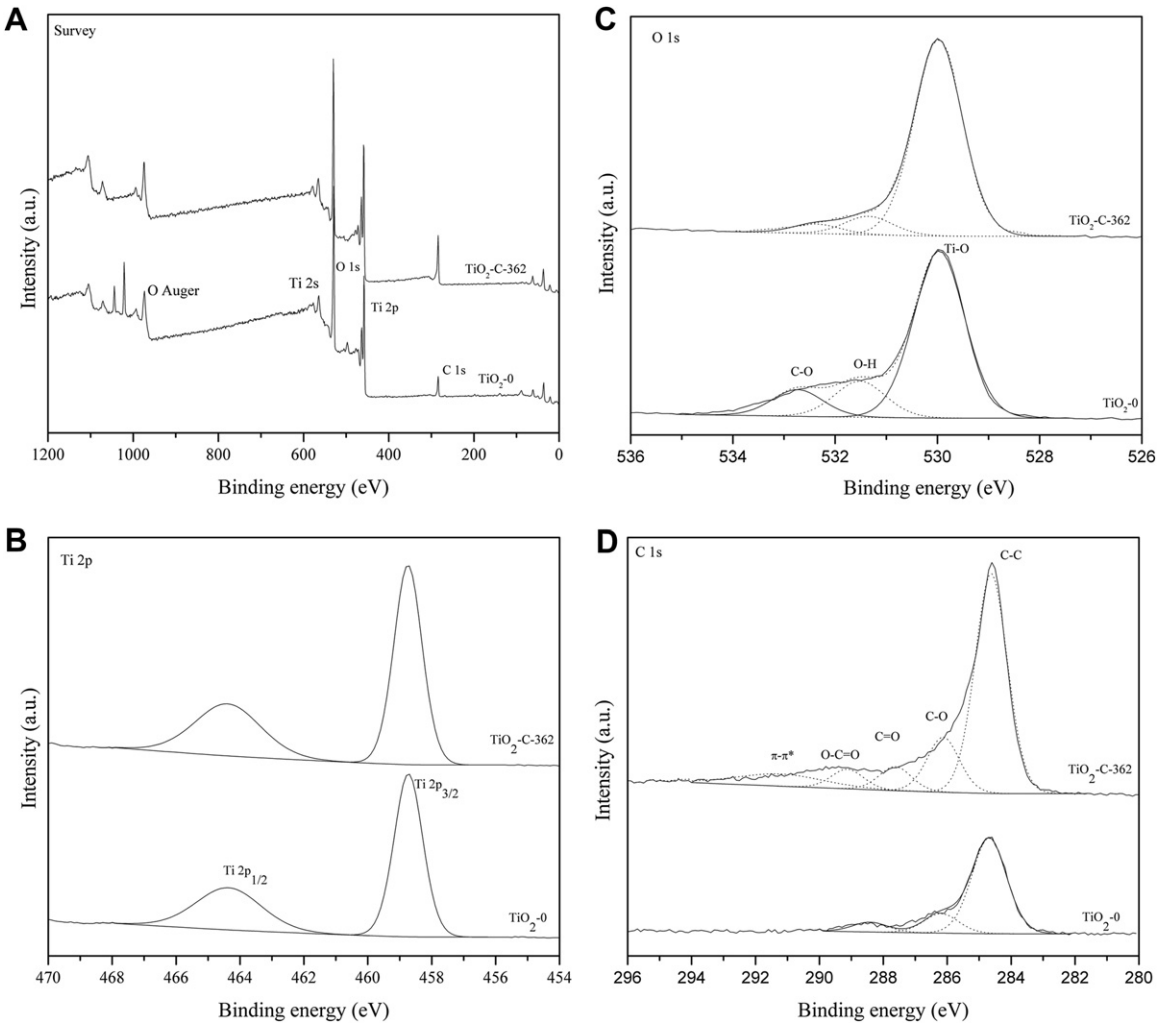

Fig. 5 – XPS results of TiO_2-C-362 and bare TiO_2-0. (A) Survey scan spectra of C-modified TiO_2 composite representative sample TiO_2-C-362 and bare TiO_2-0. (B) High resolution XPS Ti 2*p* region. (C) O 1*s* region, and (D) C 1*s* region.

the photogenerated holes are capable of oxidizing methanol in two ways. The first method involves direct oxidation, while the second method involves the formation of hydroxyl radicals *via* the reaction of water molecules and holes. The hydroxyl radicals may then react with methanol and form hydroxymethyl radicals. In the absence of dissolved oxygen [58,59], the hydroxymethyl radical may inject additional electrons into the TiO_2 conduction band. The conduction band edge of anatase, is −0.57 V vs NHE [60], while that of rutile is −0.34 V vs NHE [61]. Our experiments were performed under solar simulated conditions and the UV component of the solar light would have provided sufficient energy for electrons to be promoted to the conduction band edge of anatase which lie at more negative values compared to the H^+/H_2 redox potential. The electrons can then migrate to the conduction band edge of rutile. Additional electrons may be injected into the conduction band of rutile *via* the mechanism discussed previously. Besides mixed phases, the presence of carbon may facilitate the electron transfer and reduce the electron–hole recombination and increase the production of hydrogen. Our powder XRD results indicate that the inactive material, TiO_2-0 contains ca. 5% anatase, whereas only purely rutile phase is obtained for the material pyrolyzed under N_2 flow (TiO_2-0-N). As the carbon content is increased to 0.79% and 1.20% respectively, in the samples TiO_2-C-79 and TiO_2-C-120, the H_2 evolution increases to 0.05 and 0.10 mL/h/g_{TiO2} respectively. The highest H_2 production in this study was achieved from the carbon composite material, TiO_2-C-362, evolving 0.21 mL/h/g_{TiO2} after 6 h of irradiation. This may be attributed to optimum C loading that favors efficient electron transfer to the shallow trapped states and minimized charge carrier recombination. A further increase in carbonization to 4.02% resulted in the reduction in activity of the composites as suggested by the 0.05 mL/h/g_{TiO2} of hydrogen evolved from TiO_2-C-402 in the same time interval. Carbon modification appears to play a vital role in enhancing the activity towards photocatalytic water splitting. The high activity of TiO_2-C-362 may be attributed to a combination of factors that include high surface area, large pore volume, and most importantly effective trapping of the electrons in the shallow traps associated with oxygen vacancies (formed in the bulk or surface of TiO_2) and minimizing electron–hole recombination. It has

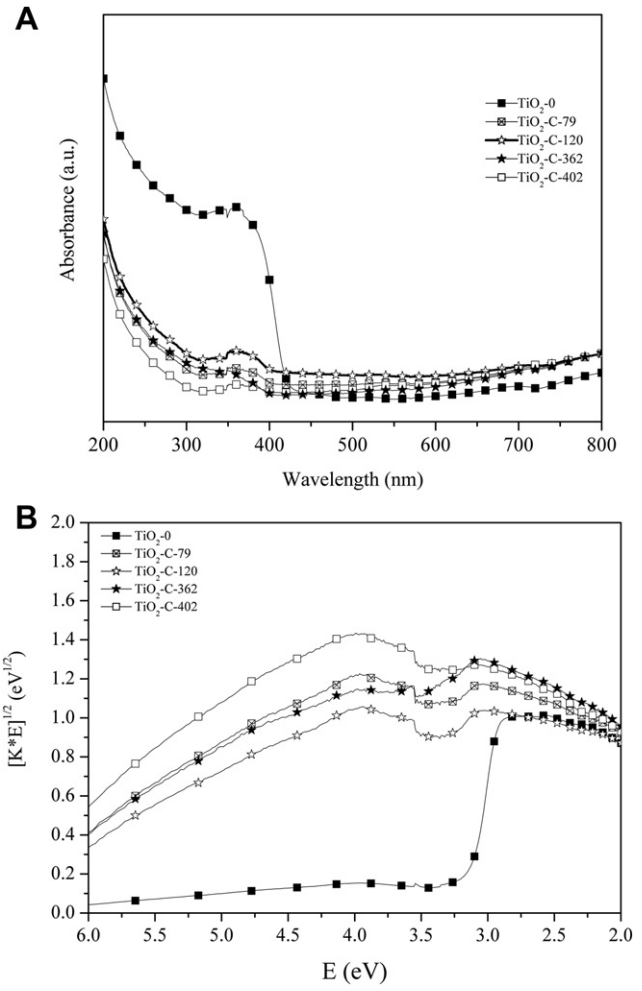

Fig. 6 – (A) Diffuse Reflectance spectra and (B) corresponding Kubelka–Munk plot for bare TiO_2-0 and C-modified TiO_2 composites.

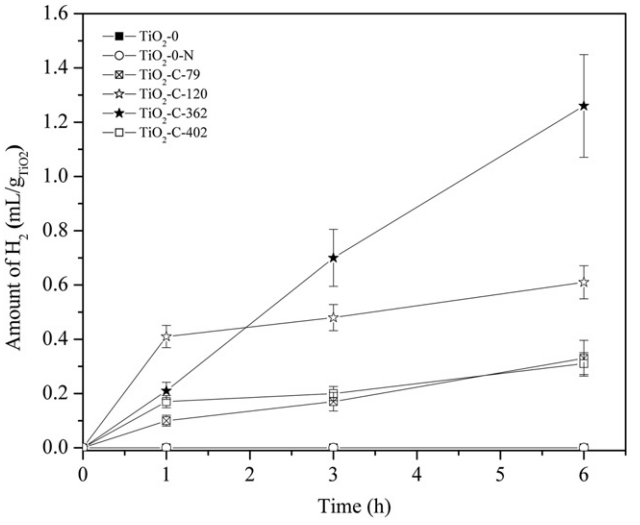

Fig. 7 – Photocatalytic hydrogen evolution from C-modified TiO_2 composite materials. Bare TiO_2-0 and TiO_2 pyrolyzed under N_2 atmosphere (TiO_2-0-N) are also shown for comparison.

been acknowledged that at higher carbon contents, more oxygen vacancies that can populate impurity states and suppress photocatalytic activity [28] and this may account for the lower activity of TiO_2-C-402. To understand the high activity of the sample TiO_2-C-362, and the nature of the electron–hole recombination, PL studies were carried out.

3.8. *Photoluminescence spectroscopy studies*

Information on the structural defects and the extent of charge carrier recombination was determined by PL studies in order to provide rationale for the photocatalytic efficiencies of the composite materials. The samples were excited at 280 nm and PL spectra were monitored in the range of 400–600 nm as depicted in Fig. 8. The wavelengths corresponding to various transitions were calculated based on the Daude model [62]. The differences in energy of the trap levels identified in these spectra at 504 nm and 586 nm are attributed to Ti^{4+} ions adjacent to oxygen vacancies (intra gap surface states) [63]. The surface emissions at 440, 451, and 467 nm are attributed to indirect transition X_{1a} to Γ_{1b} and linked to exciton recombination in shallow trapped surface states [62]. Other surface emissions observed at 482 and 492 nm are attributed to defect levels of coordinately unsaturated ions such as Ti^{3+} incorporated OH [62–65]. The high PL intensity of bare TiO_2-0 is indicative of emissions resulting from electron–hole recombination whereas the low PL intensity of the TiO_2-C-362 composite material implies enhanced separation of electron–hole pairs due to carbon modification. This phenomenon was explained by Di Valentin et al. [66] who theorized that carbon modification may favor the formation of oxygen vacancies that trap electrons resulting in a decreased PL intensity [28]. It is imperative to acknowledge the contribution of carbon to charge separation in TiO_2, as it is facilitates efficient electron trapping resulting from doping or surface modification. In photocatalytic water splitting, photogenerated electrons could transfer from the conduction band of TiO_2 to water *via* shallow trap states, and effectively

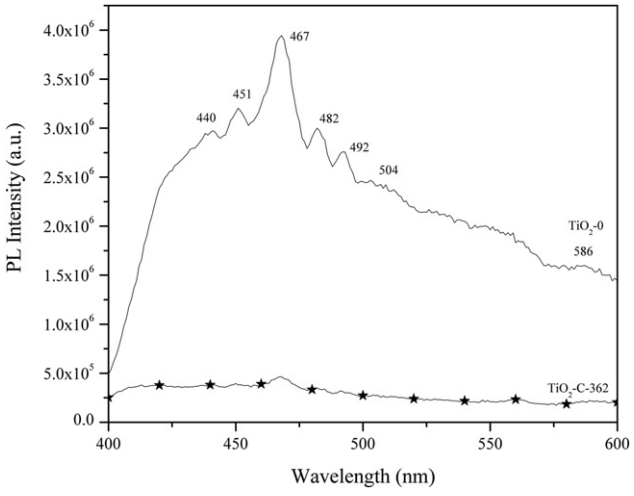

Fig. 8 – PL spectra of bare TiO_2-0 and a representative of the C-modified TiO_2 composites, TiO_2-C-362. The excitation wavelength used was 280 nm.

suppress the charge recombination at an optimum carbon content resulting in higher hydrogen evolution efficiencies.

4. Conclusions

We prepared highly active mesoporous C-modified TiO_2 composite materials from the pyrolysis of hydrothermally synthesized sucrose–TiO_2. The resultant materials exhibited high photocatalytic activity for the evolution of hydrogen under solar simulated irradiation conditions. H_2 production was achieved from the C-modified composites evolving at rates as high as 1.25 mL h^{-1} from 0.002 g of catalyst after 6 h of irradiation. The optimum loading at 3.62% of mesoporous carbon allows efficient electron trapping in shallow states thereby enabling effective separation of the charge carriers and promoting improved photocatalytic water splitting. This work provides information for the environmental friendly synthesis of carbon based nanocomposites and utilization of such materials for alternative fuel generation, and for the degradation of organic pollutants.

Acknowledgement

This work was supported by DE-EE 0000270, NSF-CHE 0840507, NSF-CHE 0722632, and NSF-EPS 0903804. We are thankful to Dr. C.Y. Jiang for help with Raman spectroscopy analysis, and Dr. C. Lin for TEM analysis. The authors also acknowledge Mr. Tyler Bloch for assistance with the synthesis of material, Mr. C. Bruce Gray for C, H, N analysis, and Prof. V.H. Grassian for assistance with XPS studies.

REFERENCES

[1] Muradov NZ, Veziroğlu TN. “Green” path from fossil-based to hydrogen economy: an overview of carbon-neutral technologies. International Journal of Hydrogen Energy 2008; 33:6804–39.
[2] Ishibashi K-I, Fujishima A, Watanabe T, Hashimoto K. Quantum yields of active oxidative species formed on TiO_2 photocatalyst. Journal of Photochemistry and Photobiology A: Chemistry 2000;134:139–42.
[3] Hagfeldt A, Graetzel M. Light-induced redox reactions in nanocrystalline systems. Chemical Reviews 1995;95:49–68.
[4] Viticoli M, Curulli A, Cusma A, Kaciulis S, Nunziante S, Pandolfi L, et al. Third-generation biosensors based on TiO_2 nanostructured films. Materials Science and Engineering: C 2006;26:947–51.
[5] Yoon M, Chang JA, Kim Y, Choi JR, Kim K, Lee SJ. Heteropoly acid-incorporated TiO_2 colloids as novel photocatalytic systems resembling the photosynthetic reaction center. The Journal of Physical Chemistry B 2001;105:2539–45.
[6] Fujishima A, Honda K. Electrochemical photolysis of water at a semiconductor electrode. Nature 1972;238:37–8.
[7] Mills A, Le Hunte S. An overview of semiconductor photocatalysis. Journal of Photochemistry and Photobiology A: Chemistry 1997;108:1–35.
[8] Lightcap IV, Kosel TH, Kamat PV. Anchoring semiconductor and metal nanoparticles on a two-dimensional catalyst mat. storing and shuttling electrons with reduced graphene oxide. Nano Letters 2010;10:577–83.
[9] Peng T, Hasegawa A, Qiu J, Hirao K. Fabrication of titania tubules with high surface area and well-developed mesostructural walls by surfactant-mediated templating method. Chemistry of Materials 2003;15:2011–6.
[10] Martin ST, Morrison CL, Hoffmann MR. Photochemical mechanism of size-quantized vanadium-doped TiO_2 particles. The Journal of Physical Chemistry 1994;98: 13,695–13,704.
[11] Choi W, Termin A, Hoffmann MR. The role of metal ion dopants in quantum-sized TiO_2: correlation between photoreactivity and charge carrier recombination dynamics. The Journal of Physical Chemistry 1994;98:13,669–13,679.
[12] Xu J, Ao Y, Chen M, Fu D. Low-temperature preparation of boron-doped titania by hydrothermal method and its photocatalytic activity. Journal of Alloys and Compounds 2009;484:73–9.
[13] Xu J, Ao Y, Fu D, Yuan C. Low-temperature preparation of F-doped TiO_2 film and its photocatalytic activity under solar light. Applied Surface Science 2008;254:3033–8.
[14] Ma Y, Fu J-W, Tao X, Li X, Chen J-F. Low temperature synthesis of iodine-doped TiO_2 nanocrystallites with enhanced visible-induced photocatalytic activity. Applied Surface Science 2011;257:5046–51.
[15] Cui X, Ma M, Zhang W, Yang Y, Zhang Z. Nitrogen-doped TiO_2 from TiN and its visible light photoelectrochemical properties. Electrochemistry Communications 2008;10: 367–71.
[16] Qiao M, Wu S, Chen Q, Shen J. Novel triethanolamine assisted sol–gel synthesis of N-doped TiO_2 hollow spheres. Materials Letters 2010;64:1398–400.
[17] Periyat P, Pillai SC, McCormack DE, Colreavy J, Hinder SJ. Improved high-temperature stability and sun-light-driven photocatalytic activity of sulfur-doped anatase TiO_2. The Journal of Physical Chemistry C 2008;112:7644–52.
[18] Ang T, Law J, Han Y-F. Preparation, characterization of sulfur-doped nanosized TiO_2 and photocatalytic degradation of methylene blue under visible light. Catalysis Letters 2010; 139:77–84.
[19] Ren W, Ai Z, Jia F, Zhang L, Fan X, Zou Z. Low temperature preparation and visible light photocatalytic activity of mesoporous carbon-doped crystalline TiO_2. Applied Catalysis B: Environmental 2007;69:138–44.
[20] Xing M-Y, Qi D-Y, Zhang J-L, Chen F. One-step hydrothermal method to prepare carbon and lanthanum Co-doped TiO_2 nanocrystals with exposed {001} facets and their high UV and visible-light photocatalytic activity. Chemistry – A European Journal 2011;17:11,432–11,436.
[21] Khan SUM, Al-Shahry M, Ingler WB. Efficient photochemical water splitting by a chemically modified n-TiO_2. Science 2002;297:2243–5.
[22] Park JH, Kim S, Bard AJ. Novel carbon-doped TiO_2 nanotube arrays with high aspect ratios for efficient solar water splitting. Nano Letters 2005;6:24–8.
[23] Chen D, Jiang Z, Geng J, Wang Q, Yang D. Carbon and nitrogen co-doped TiO_2 with enhanced visible-light photocatalytic activity. Industrial & Engineering Chemistry Research 2007;46:2741–6.
[24] Sakthivel S, Kisch H. Daylight photocatalysis by carbon-modified titanium dioxide. Angewandte Chemie International Edition 2003;42:4908–11.
[25] Janus M, Tryba B, Inagaki M, Morawski AW. New preparation of a carbon-TiO_2 photocatalyst by carbonization of *n*-hexane deposited on TiO_2. Applied Catalysis B: Environmental 2004; 52:61–7.
[26] Gu D-E, Lu Y, Yang B-C, Hu Y-D. Facile preparation of micro-mesoporous carbon-doped TiO_2 photocatalysts with anatase

crystalline walls under template-free condition. Chemical Communications; 2008:2453–5.
[27] Kim M, Kim K-D, Tai W, Seo H, Luo Y, Kim Y, et al. Enhancement of photocatalytic activity of TiO_2 by high-energy electron-beam treatment under atmospheric pressure. Catalysis Letters 2010;135:57–61.
[28] Dong F, Wang H, Wu Z. One-step "green" synthetic approach for mesoporous C-doped titanium dioxide with efficient visible light photocatalytic activity. The Journal of Physical Chemistry C 2009;113:16,717–16,723.
[29] Dong F, Guo S, Wang H, Li X, Wu Z. Enhancement of the visible light photocatalytic activity of C-doped TiO_2 nanomaterials prepared by a green synthetic approach. The Journal of Physical Chemistry C 2011;115:13,285–13,292.
[30] Zhang L-W, Fu H-B, Zhu Y-F. Efficient TiO_2 photocatalysts from surface hybridization of TiO_2 particles with graphite-like carbon. Advanced Functional Materials 2008;18:2180–9.
[31] Zhao L, Chen X, Wang X, Zhang Y, Wei W, Sun Y, et al. One-step solvothermal synthesis of a carbon@TiO_2 dyade structure effectively promoting visible-light photocatalysis. Advanced Materials 2010;22:3317–21.
[32] Li Y, Lu G, Li S. Photocatalytic hydrogen generation and decomposition of oxalic acid over platinized TiO_2. Applied Catalysis A: General 2001;214:179–85.
[33] Jin Z, Zhang X, Li Y, Li S, Lu G. 5.1% Apparent quantum efficiency for stable hydrogen generation over eosin-sensitized CuO/TiO_2 photocatalyst under visible light irradiation. Catalysis Communications 2007;8:1267–73.
[34] Li Y, Ma G, Peng S, Lu G, Li S. Boron and nitrogen co-doped titania with enhanced visible-light photocatalytic activity for hydrogen evolution. Applied Surface Science 2008;254:6831–6.
[35] Li Y, Hu Y, Peng S, Lu G, Li S. Synthesis of CdS nanorods by an ethylenediamine assisted hydrothermal method for photocatalytic hydrogen evolution. The Journal of Physical Chemistry C 2009;113:9352–8.
[36] Li Y, Du J, Peng S, Xie D, Lu G, Li S. Enhancement of photocatalytic activity of cadmium sulfide for hydrogen evolution by photoetching. International Journal of Hydrogen Energy 2008;33:2007–13.
[37] Zhao D, Budhi S, Rodriguez A, Koodali RT. Rapid and facile synthesis of Ti-MCM-48 mesoporous material and the photocatalytic performance for hydrogen evolution. International Journal of Hydrogen Energy 2010;35:5276–83.
[38] Sevilla M, Fuertes AB. The production of carbon materials by hydrothermal carbonization of cellulose. Carbon 2009;47:2281–9.
[39] Liu M, Wang C, Wang X. Interface-facilitated hydrothermal synthesis of sub-micrometre graphitic carbon plates. Journal of Materials Chemistry 2011;21:15,197–15,200.
[40] Sun X, Li Y. Colloidal carbon spheres and their core/shell structures with noble-metal nanoparticles. Angewandte Chemie International Edition 2004;43:597–601.
[41] Zhu K, Egeblad K, Christensen CH. Mesoporous carbon prepared from carbohydrate as hard template for hierarchical zeolites. European Journal of Inorganic Chemistry 2007;2007:3955–60.
[42] Lei Z, Xiao Y, Dang L, You W, Hu G, Zhang J. Nickel-catalyzed fabrication of SiO_2, TiO_2/graphitized carbon, and the resultant graphitized carbon with periodically macroporous structure. Chemistry of Materials 2006;19:477–84.
[43] Kruk M, Jaroniec M. Gas adsorption characterization of ordered organic–inorganic nanocomposite materials. Chemistry of Materials 2001;13:3169–83.
[44] Kang SH, Kim J-Y, Kim Y-K, Sung Y-E. Effects of the incorporation of carbon powder into nanostructured TiO_2 film for dye-sensitized solar cell. Journal of Photochemistry and Photobiology A: Chemistry 2007;186:234–41.
[45] Lu L, Zhu Y, Li F, Zhuang W, Chan KY, Lu X. Carbon titania mesoporous composite whisker as stable supercapacitor electrode material. Journal of Materials Chemistry 2010;20:7645–51.
[46] Sadezky A, Muckenhuber H, Grothe H, Niessner R, Pöschl U. Raman microspectroscopy of soot and related carbonaceous materials: spectral analysis and structural information. Carbon 2005;43:1731–42.
[47] Briggs D, Seah MP. Practical surface analysis by Auger and X-ray photoelectron spectroscopy; 1983.
[48] Nishimiya K, Hata T, Imamura Y, Ishihara S. Analysis of chemical structure of wood charcoal by X-ray photoelectron spectroscopy. Journal of Wood Science 1998;44:56–61.
[49] Xie Y, Sherwood PMA. X-ray photoelectron-spectroscopic studies of carbon fiber surfaces. 11. Differences in the surface chemistry and bulk structure of different carbon fibers based on poly(acrylonitrile) and pitch and comparison with various graphite samples. Chemistry of Materials 1990;2:293–9.
[50] Moser J, Punchihewa S, Infelta PP, Graetzel M. Surface complexation of colloidal semiconductors strongly enhances interfacial electron-transfer rates. Langmuir 1991;7:3012–8.
[51] Kim S, Choi W. Visible light-induced photocatalytic degradation of 4-chlorophenol and phenolic compounds in aqueous suspension of pure titania: demonstrating the existence of a surface-complex-mediated path. The Journal of Physical Chemistry B 2005;109:5143–9.
[52] Rajh T, Chen LX, Lukas K, Liu T, Thurnauer MC, Tiede DM. Surface restructuring of nanoparticles: an efficient route for ligand–metal oxide crosstalk. The Journal of Physical Chemistry B 2002;106:10,543–10,552.
[53] Rajh T, Nedeljkovic JM, Chen LX, Poluektov O, Thurnauer MC. Improving optical and charge separation properties of nanocrystalline TiO_2 by surface modification with vitamin C. The Journal of Physical Chemistry B 1999;103:3515–9.
[54] Dimitrijevic NM, Saponjic ZV, Bartels DM, Thurnauer MC, Tiede DM, Rajh T. Revealing the nature of trapping sites in nanocrystalline titanium dioxide by selective surface modification. The Journal of Physical Chemistry B 2003;107:7368–75.
[55] Dimitrijevic NM, Rajh T, Saponjic ZV, de la Garza L, Tiede DM. Light-induced charge separation and redox chemistry at the surface of TiO_2/host–guest hybrid nanoparticles. The Journal of Physical Chemistry B 2004;108:9105–10.
[56] Dimitrijevic NM, Rozhkova E, Rajh T. Dynamics of localized charges in dopamine-modified TiO_2 and their effect on the formation of reactive oxygen species. Journal of the American Chemical Society 2009;131:2893–9.
[57] Kho YK, Iwase A, Teoh WY, Madler L, Kudo A, Amal R. Photocatalytic H_2 evolution over TiO_2 nanoparticles. The synergistic effect of anatase and rutile. The Journal of Physical Chemistry C 2010;114:2821–9.
[58] Teoh WY, Mädler L, Amal R. Inter-relationship between Pt oxidation states on TiO_2 and the photocatalytic mineralisation of organic matters. Journal of Catalysis 2007;251:271–80.
[59] Wang C-Y, Pagel R, Bahnemann DW, Dohrmann JK. Quantum yield of formaldehyde formation in the presence of colloidal TiO_2-based photocatalysts:Effect of intermittent illumination, platinization, and deoxygenation. The Journal of Physical Chemistry B 2004;108:14,082–14,092.
[60] Kavan L, Grätzel M, Gilbert SE, Klemenz C, Scheel HJ. Electrochemical and photoelectrochemical investigation of single-crystal anatase. Journal of the American Chemical Society 1996;118:6716–23.
[61] Kalyanasundaram K, Grätzel M. Applications of functionalized transition metal complexes in photonic and optoelectronic devices. Coordination Chemistry Reviews 1998;177:347–414.

[62] Daude N, Gout C, Jouanin C. Electronic band structure of titanium dioxide. Physical Review B 1977;15:3229–35.
[63] Ghosh AK, Wakim FG, Addiss Jr RR. Photoelectronic processes in rutile. Physical Review 1969;184:979–88.
[64] Kumar PM, Badrinarayanan S, Sastry M. Nanocrystalline TiO_2 studied by optical, FTIR and X-ray photoelectron spectroscopy: correlation to presence of surface states. Thin Solid Films 2000;358:122–30.
[65] Jang JH, Jeon KS, Park TS, Lee KW, Yoon M. Formation of trititanate nanotubes by non-hydrothermal methods: optical properties and surface-exciton dynamics studied by photoluminescence spectroscopy. Journal of the Chinese Chemical Society 2006;53:123–30.
[66] Di Valentin C, Pacchioni G, Selloni A. Theory of carbon doping of titanium dioxide. Chemistry of Materials 2005;17:6656–65.